


## Asymmetric lateral sound beaming in a Willis medium

Xiaoshi Su \* and Debasish Banerjee

Toyota Research Institute of North America, 1555 Woodridge Avenue, Ann Arbor, Michigan 48105, USA

 (Received 18 April 2021; revised 6 July 2021; accepted 8 July 2021; published 22 July 2021)

Willis coupling, also known as pressure-velocity cross coupling, in acoustic materials has received much attention in the past years. This effect has been found useful in acoustic metasurface designs for wave redirection. We find that Willis coupling in phononic crystals also provides rich physics to manipulate waves. Here, we report the extreme asymmetric lateral sound beaming effect in a two-dimensional phononic crystal composed of Willis scatterers. By matching the second-order Bragg scattering with two leaky guided modes (a quadrupole resonance and a cross-coupling-induced dipole resonance), a normally incident wave is redirected towards the positive and negative directions orthogonal to the incident wave with different amounts of energy. Simulation and experimental results demonstrate the extraordinary asymmetric lateral beaming effect in the Willis medium. The results presented here may find applications in the design of tunable beam splitters and waveguides.

DOI: [10.1103/PhysRevResearch.3.033080](https://doi.org/10.1103/PhysRevResearch.3.033080)

### I. INTRODUCTION

Willis materials are composite materials displaying cross coupling between strain and momentum [1]. The cross-coupling effect is often referred to as the Willis coupling and usually occurs in inhomogeneous materials [2]. Much effort has been made to understand the effect of Willis coupling in elastodynamics [2–5]. Willis coupling also exists in some acoustic media in which the acoustic pressure couples to the particle velocity [2,5,6]. It is also found that Willis coupling is analogous to the bianisotropy in electromagnetism [2,7]. Hence Willis materials are sometimes also referred to as bianisotropic materials. Various applications have been reported in elastodynamics, such as nonreciprocal transmission in an active Willis material [8], asymmetric absorption and scattering in a passive Willis material [9], and simultaneous control of transmitted and reflected waves using active Willis materials [10]. Highly efficient acoustic metasurfaces [11] and metagratings [12–16] for sound redirection based on Willis coupling have been reported. Unidirectional zero reflection and nonreciprocal transmission of sound have also been demonstrated in Willis materials [17,18].

In this paper, we report an extraordinary lateral sound beaming effect in a Willis medium (phononic crystal composed of Willis scatterers arranged in a square lattice pattern). It should be noted that the special scattering properties of the Willis scatterers are crucial to the realization of the asymmetric lateral sound beaming effect. For a conventional

acoustic scatterer, the monopole response (scalar) can only be generated by the acoustic pressure (scalar), while the dipole response (vector) can only be generated by the velocity (vector). However, due to the cross coupling between pressure and velocity, Willis scatterers can also display dipole response under pressure excitation and display monopole response under velocity excitation [12]. Previously reported lateral sound beaming effects in phononic crystals are based on the quadrupole mode, which is symmetric, in the unit cell [19–21]. Therefore, the transmitted beams in the lateral directions are always symmetric. By using Willis scatterers in the phononic crystal, the pressure excited dipole moment in the unit cell forms an additional antisymmetric mode orthogonal to the incident wave. By matching the antisymmetric and symmetric modes to the second-order Bragg scattering in the Willis medium, the asymmetric lateral beaming effect is possible.

### II. PHONONIC CRYSTAL COMPOSED OF WILLIS SCATTERERS

The Willis medium for asymmetric lateral beaming proposed in this paper is depicted in Fig. 1. Multiple Willis scatterers are arranged in a square lattice manner with lattice constant  $d$  as shown in Fig. 1(a). The acoustic medium surrounding the Willis medium is air, and all the scatterers are considered acoustically rigid. Figure 1(b) shows the geometric parameters of the scatterer in which the inner radius is denoted by  $r_i$ , the outer radius is denoted by  $r_o$ , and the neck width is denoted by  $w$ . The sound beaming effect is illustrated in Fig. 1(a): A plane wave is normally incident along the  $+y$  direction; the wave is then partially reflected along the  $-y$  direction and partially transmitted through two lateral directions along the  $\pm x$  axis as well as the  $+y$  direction. The extreme case of particular interest in this paper is that the energy transmission towards the  $+x$  direction is much larger than that towards the  $-x$  direction. However,

\*xiaoshi.su@toyota.com

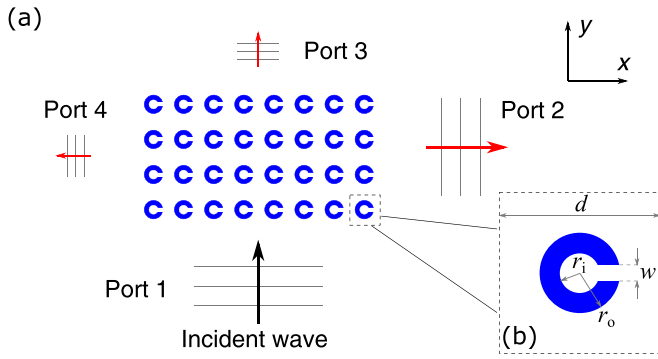


FIG. 1. Description of the Willis medium. The material is composed of Willis scatterers arranged in a square lattice pattern as shown in (a). A plane wave is normally incident along the  $+y$  direction from port 1; the transmitted waves can exit from ports 2, 3, and 4. (b) shows the details of the unit cell. The lattice constant is denoted by  $d$ ;  $r_i$ ,  $r_o$ , and  $w$  are the inner radius, outer radius, and neck width, respectively.

the scattered waves from conventional scatterers are always symmetric about the incident direction. Therefore, although conventional phononic crystals can split waves towards the lateral directions, the lateral beaming effect is always symmetric [19–21].

In order to achieve the asymmetric lateral beaming effect, the scattered waves from the scatterers must contain asymmetric components. Recent research on Willis acoustic scatterers provides a means of generating the dipole moment orthogonal to the incident direction [12,22]. It is found that the acoustic pressure can excite a dipole moment orthogonal to the incident direction due to the cross coupling between acoustic pressure and particle velocity. This effect has been utilized to achieve wave cancellation with monopole response in a metagrating design [12]. In this paper, we consider a higher frequency range ( $ka \sim 1$ , where  $k$  is the wave number and  $a = r_o$ ) in a phononic crystal and utilize the pressure excited dipole together with a quadrupole response to achieve the asymmetric lateral beaming outlined in this paper. The dipole scattering properties of the Willis scatterer designed in this paper along the orthogonal direction are studied and presented in Fig. 2. The acoustic medium surrounding the scatterer is air with Bulk modulus  $B = 1.42$  MPa and mass density  $\rho = 1.204$  kg/m<sup>3</sup>; the scatterer is considered to be acoustically rigid. The scattering coefficients  $|\alpha'|$  shown in Fig. 2 are calculated using the method described in Ref. [22]. Figure 2(a) shows the dipole scattering coefficients along the  $x$  direction for a wave incident along the  $\pm y$  direction. The results for a rigid cylinder of the same radius are also plotted for comparison. Obviously, the pressure excited dipole moment (orthogonal to the incident direction) from the Willis scatterer is more than five orders of magnitude higher than that from a rigid cylinder. This difference is due to the fact the Willis scatterer is asymmetric about the  $y$  axis which caused the pressure-velocity cross coupling. The geometric parameters of the scatterer are important to the dipole scattering strength under pressure excitation. Due to the asymmetric internal structure, the dipole scattering coefficient corresponding to the pressure excited dipole ( $|\alpha_x^{pv}|$ )

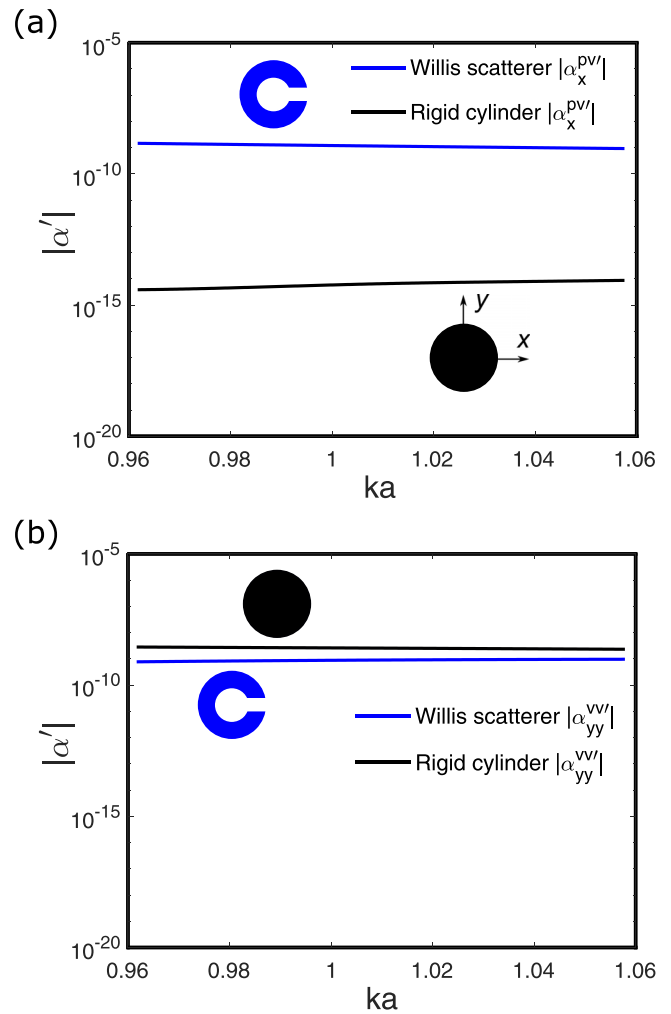


FIG. 2. Normalized dipole scattering coefficients for a normally incident plane wave along the  $+y$  direction. (a) corresponds to the acoustic pressure excited dipole orthogonal to the direction of the incident wave. (b) corresponds to the acoustic velocity excited dipole along the incident direction. The blue and black lines represent the dipole scattering coefficients for the C-shaped scatterer and a rigid scatterer of the same outer radius, respectively.

orthogonal to the incident direction is significantly increased. Although not shown in Fig. 2, the maximum scattering of the pressure excited dipole occurs near the resonant frequency around  $ka \approx 0.77$  and gradually decreases at higher or lower frequencies. The resonant frequency is determined by the geometric parameters of the scatterer. One can increase the inner radius  $r_i$  or reduce the neck width  $w$  to decrease the resonant frequency. One can also reduce the inner radius or increase the neck width to increase the resonant frequency. The objective of this paper is not to achieve maximum cross coupling, and its frequency actually lies outside the frequency range of interest. However, it is remarkable that the cross-coupling-induced dipole is still not perturbative at non-resonant frequencies in our design. In fact, the strength of the pressure excited dipole orthogonal to the incident direction is comparable to the strength of the velocity excited dipole along the incident direction as shown in Fig. 2(b). By taking advantage of the cross coupling in the Willis material,

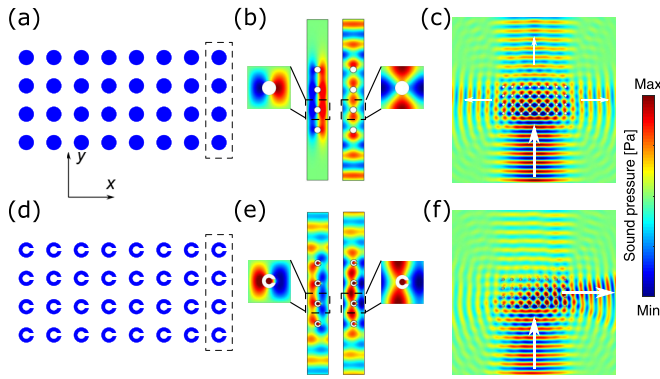


FIG. 3. Lateral beaming in periodic structures. (a) is a square lattice of rigid cylinders; the radius of each cylinder is  $r = 1.05$  cm, and the lattice constant is  $d = 6.466$  cm. (b) illustrates the first anti-symmetric (4924.9 Hz) and symmetric ( $5283.9 + 173.39i$  Hz) modes and the corresponding dipole and quadrupole modes in the unit cell. (c) is the simulated sound pressure field at 5305 Hz showing the symmetric lateral beaming effect in the periodic structure; a Gaussian beam is normally incident along the  $+y$  direction. (d) is a Willis medium composed of C-shaped scatterers; the outer radius of the scatterer is  $r_o = 1.05$  cm, and the lattice constant is  $d = 6.466$  cm. (e) shows the two modes similar to those in (b) at two different frequencies ( $5158.3 + 81.583i$  Hz and  $5280.4 + 71.982i$  Hz) and the corresponding dipole and quadrupole modes in the unit cell. The simulated asymmetric lateral beaming in a Willis medium at 5305 Hz is shown in (f).

the asymmetric lateral beaming effect proposed in Fig. 1 is possible.

### III. ASYMMETRIC LATERAL SOUND BEAMING

#### A. Lateral sound beaming in a phononic crystal

Previously reported lateral beaming effects for sound waves in water and flexural waves in plates are all symmetric [19–21]. The reason is that the conventional scatterers in those designs are nonbianisotropic (no Willis coupling), so that the antisymmetric modes inside the phononic crystal cannot be excited. Here, we begin with the symmetric lateral sound beaming effect in air and then show that the symmetry can be broken by using Willis scatterers. As shown in Fig. 3(a), a cluster of rigid cylinders ( $8 \times 4$  array) with radius  $r = 1.05$  cm are arranged in a square lattice pattern with a lattice constant  $d = 6.466$  cm.

For a phononic crystal, the strongest scattering occurs when the Bragg condition  $n\lambda = 2d \sin \theta$  is satisfied, where  $n$  is a positive integer,  $\theta$  is the incident angle, and  $\lambda$  is the wavelength. For this specific case in which the sound is normally incident ( $\theta = 90^\circ$ ), the second-order Bragg scattering ( $n = 2$ ) occurs at 5305 Hz. By tuning the radius  $r$  of the cylinder, the resonant modes inside the phononic crystal can be adjusted to match the Bragg scattering. The first antisymmetric and symmetric modes for  $r = 1.05$  cm are displayed in Fig. 3(b). Here, a mode is called symmetric when the mode shape is symmetric about the centerline along the  $y$  direction and is called antisymmetric when the mode shape is antisymmetric about the centerline along the  $y$  direction. The antisymmetric mode at 4924.9 Hz is a dipole mode in the unit cell, which cannot be excited by a normally incident sound. However, the symmetric mode at  $5283.9 + 173.39i$  Hz is a quadrupole mode in the unit cell and couples to the incident wave. The

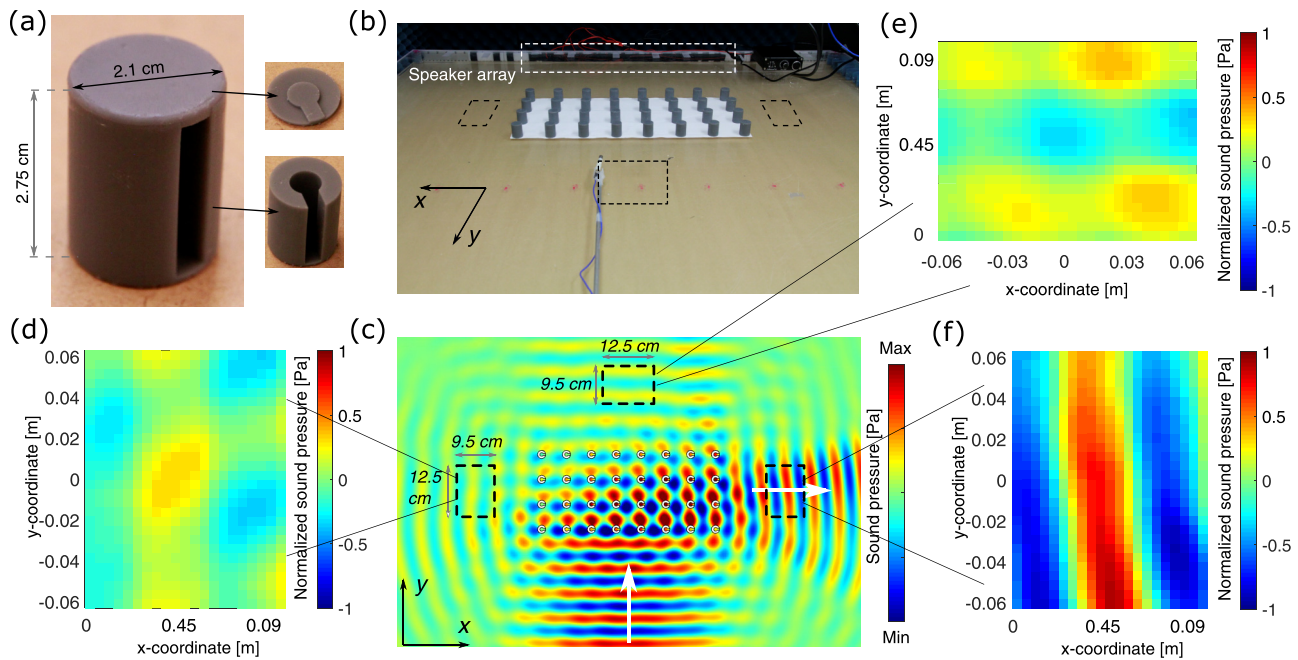


FIG. 4. Measurement results. (a) shows the three-dimensional (3D) printed Willis scatterer; (b) shows the measurement setup of the Willis media placed in a 2D waveguide (two 11/16-in.-thick acrylic plates of  $48 \times 48$ -in. size separated by 2.75 cm in parallel); the 32 scatterers are arranged in a square lattice pattern with a lattice constant of  $d = 6.466$  cm; the open necks of the scatterers are oriented towards the  $+x$  direction; sound pressure fields were measured in three  $12.5 \times 9.5$ -cm areas indicated by dashed rectangles (12 cm away from the scatterers). (c) is the simulated sound pressure field at 5305 Hz for a normally incident Gaussian beam along the  $+y$  direction; (d)–(f) are the measured sound pressure fields at 5305 Hz corresponding to the three areas in (b) and (c) marked by dashed rectangles.

insets in Fig. 3(b) illustrate the relations between the dipole mode in the unit cell and the antisymmetric mode in the scatterer array, and the relations between the quadrupole mode in the unit cell and the symmetric mode in the scatterer array. The dipole modes in the unit cells contribute to the antisymmetric mode of the scatterer array; the quadrupole modes in the unit cells contribute to the symmetric mode of the scatterer array. It is noted that the frequency of the symmetric mode not only has a real part close to 5305 Hz, but also has an imaginary component. As explained in Ref. [21], the positive imaginary part of the mode determines its lifetime. A complex resonant frequency with a large imaginary part means that the lifetime of the mode is short, which is due to more energy leakage into free space. In other words, the imaginary part of the mode leads to a substantial spatial effect of the mode, i.e., a leaky guided mode, in a finite phononic crystal. Figure 3(c) shows the simulation result obtained using COMSOL MULTIPHYSICS at 5305 Hz. It is obvious that the beams along the  $\pm x$  directions are symmetric since the quadrupole mode is symmetric.

### B. Asymmetric lateral sound beaming in a Willis medium

The redirected waves along the two lateral directions can be asymmetric in a Willis medium thanks to the acoustic pressure excited dipole moment orthogonal to the incident wave. The phononic crystal composed of Willis scatterers is shown in Fig. 3(d). The outer radius of the scatterer is  $r_o = 1.05$  cm, the inner radius is  $r_i = 0.47$  cm, and the neck width is  $w = 0.5$  cm. The lattice constant is also  $d = 6.466$  cm corresponding to second-order Bragg scattering at 5305 Hz for normally incident sound. The geometries are tailored so that the two modes shown in Fig. 3(e) are both close to 5305 Hz. The design procedure is described as follows. First, the outer radius  $r_o = 1.05$  cm is adopted from the conventional scatterer presented in Sec. III A, which is determined by varying its value to match the frequency of the symmetric mode to the second-order Bragg scattering. Then the internal structure of the C-shaped scatterer is introduced to couple the antisymmetric mode of the Willis phononic crystal to the incident wave and provide the possibility to tune the frequency. The frequency of the antisymmetric mode can be adjusted by changing the inner radius  $r_i$  and neck width  $w$ . The neck width is kept relatively large at 0.5 cm to simplify the design process and reduce the thermoviscous loss. By varying the inner radius  $r_i$ , we shifted the resonant frequency of the antisymmetric mode close to the second-order Bragg scattering. It can be easily observed from the mode shapes that they are coupled to the propagating wave along the  $y$  direction. Both of the two resonant frequencies ( $5158.3 + 81.583i$  Hz and  $5280.4 + 71.982i$  Hz) have substantial imaginary components, leading to the spatial effect along the  $x$  direction in the finite phononic crystal. Due to the symmetry (antisymmetry) of the two leaky guided modes, destructive interference along the  $-x$  direction decreases the transmission, while constructive interference along the  $+x$  direction increases the transmission. Hence the asymmetric lateral beaming effect is achieved as shown in the simulation results in Fig. 3(f).

It is also interesting to see that the transmission vanishes along the  $+y$  direction. This phenomenon is due to the interference between the incident wave and the scattered waves.

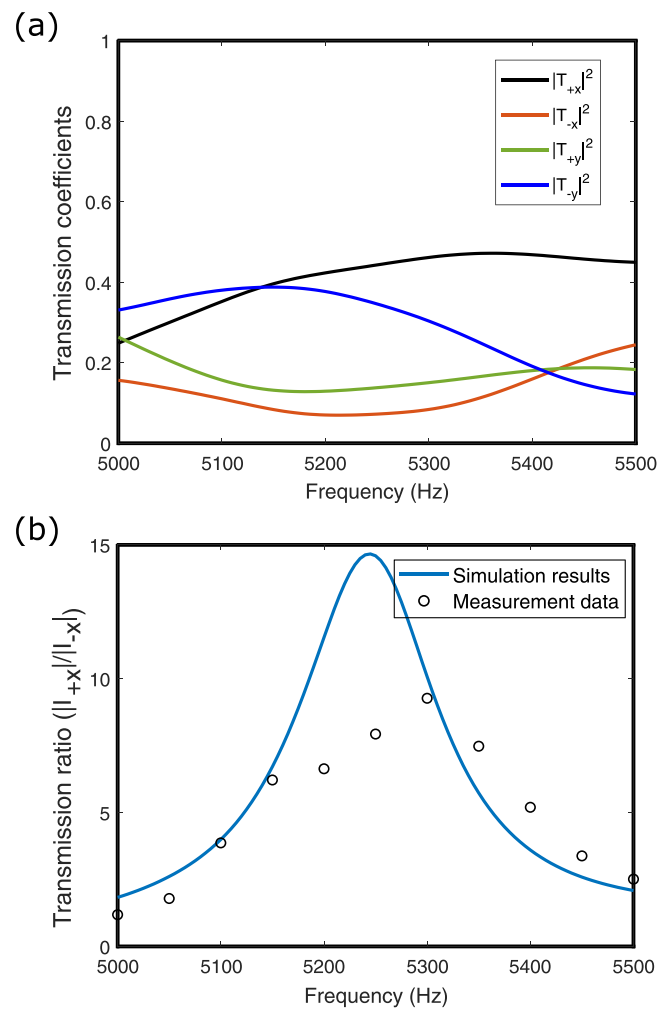


FIG. 5. Transmission properties through the Willis medium. (a) shows the transmission coefficients calculated from simulation results along the  $+y$  and  $\pm x$  directions ( $|T_{+y}|^2$  and  $|T_{\pm x}|^2$ ) and the reflection coefficient along the  $-y$  direction ( $|T_{-y}|^2$ ). A maximum transmission along the  $+x$  direction of 47.2% occurs near 5360 Hz in the simulation. (b) shows the asymmetry ratio, defined as the ratio between the sound intensity through the two dashed rectangles along the  $+x$  and  $-x$  directions in Figs. 4(b) and 4(c); the solid curve represents the simulation results, while the circles represent the measurement data. The maximum asymmetry ratio between the  $+x$  and  $-x$  directions ( $|I_{+x}|/|I_{-x}| = 9.27$ ) occurs at 5305 Hz in the measurements.

The symmetric and antisymmetric modes in Fig. 3(f) both couple to the propagating modes. Under the plane wave excitation along the  $+y$  direction, these two propagating modes are both excited. Their interference forms scattered waves from the Willis medium along the  $\pm y$  directions. Since the propagating modes in Fig. 3(f) are both symmetric about the centerline along the  $x$  direction, the waves transmitted through the  $y$  direction and the waves reflected along the  $-y$  direction are the same. The transmission along the  $+y$  direction appears small in Fig. 3(f), because the incident wave and the scattered wave along the  $+y$  direction have destructive interference at the frequency range of interest, so that the transmission vanishes. In the following section, we will calculate the energy



propagations along different directions and compare them with measurement results.

### C. Experimental results

Acoustic measurements were done to demonstrate the performance of the asymmetric lateral beaming effect. A total number of 32 scatterers were fabricated by using stereolithography of gray resin. The scatterer is fabricated in two parts with a body 2.6 cm tall and a cover 0.15 cm thick as shown in Fig. 4(a). The Young's modulus of the fabricated structure is  $E = 2.8$  GPa, and the density is  $\rho = 1.78$  kg/m<sup>3</sup>. The experimental apparatus shown in Fig. 4(b) is the same as that used in Ref. [23], except that the distance between the top and bottom plates of the waveguide is now 2.75 cm. The scatterers are arranged in a square lattice pattern with a lattice constant of  $d = 6.466$  cm. The speaker array 30 cm away from the scatterers generates a plane wave ranging from 3 to 7 kHz. Sound pressure fields were measured in three  $12.5 \times 9.5$ -cm areas as marked in Fig. 4(c). Note that Fig. 4(c) is the simulation result at 5305 Hz for reference (the same as Fig. 4). The measured pressure fields at 5305 Hz in the aforementioned three areas are plotted in Figs. 4(d)–4(f). As we can see, the simulated sound wave is incident along the  $+y$  direction and transmits through the structure along the  $+x$  direction. The measured pressure fields are normalized to the maximum amplitude in the three areas. The amplitude of the pressure field in Fig. 4(f) is significantly higher than that in Figs. 4(d) and 4(e). The results clearly show the asymmetric lateral beaming effect in the fabricated structures. To quantify the asymmetric lateral beaming effect, we calculated the simulated energy transmission and reflection coefficients along four directions ( $\pm x$  and  $\pm y$ ). The energy propagating along four directions was computed by integrating the intensity  $I$  over the four sides of the phononic crystal resulting in the energy  $E = \int I \cdot ndL$ . The results are plotted in Fig. 5(a). The maximum transmission towards the  $+x$  direction is about 47.2% at 5360 Hz. Due to the limitations of our measurement system, only limited areas along three directions were measured, so that the corresponding coefficients cannot be calculated using the measurement data. However, we directly computed the ratio of the energy flux in the  $+x$  direction to the energy flux in the  $-x$  direction using measurement data and

compared it with that calculated in the simulation. The results are presented in Fig. 5(b). The measurement result shows a maximum ratio of 9.27 at 5305 Hz between the energy transmitted in the  $+x$  direction and the energy transmitted in the  $-x$  direction. It is noted that the simulation data yield a maximum ratio of about 14.7 near 5240 Hz. The overall shapes of the two curves match well except that the simulation result has a sharper peak shifted away from 5305 Hz. The difference between the measurement data and the simulation results is likely due to the alignment error of the scatterers. The distances between the scatterers are slightly different, and their open necks are not perfectly oriented towards the  $+x$  direction, which may reduce the Bragg scattering and the strength of the resonant modes. Another reason is that the pressure field is not evenly distributed along the  $y$  axis; more energy may be redirected to areas near the dashed rectangular areas and change the energy flux ratio in the measurement results. Other than the aforementioned discrepancy, our design shows a broadband asymmetric lateral beaming effect with an energy transmission ratio of at least 5 within 5125–5400 Hz.

### IV. CONCLUSIONS

In conclusion, we presented an extraordinary asymmetric lateral beaming effect in a phononic crystal composed of Willis scatterers arranged in a square lattice manner. The asymmetric lateral beaming effect is achieved by matching the dipole and quadrupole modes with Bragg scattering, where the dipole response orthogonal to the incident wave is excited by the pressure field. The wave numbers of the aforementioned two modes both have relatively large imaginary components and hence display a spatial effect as leaky guided modes. Furthermore, the interference between the symmetric and antisymmetric modes causes asymmetry in the transmission pattern. The experimental results presented in this paper show a maximum intensity ratio of 9.27 at the design frequency. In addition, the structures can be easily rotated so that the maximum transmission direction can be easily switched towards other directions. We envision future applications in beam splitter and waveguide designs.

- 
- [1] J. R. Willis, Variational principles for dynamic problems for inhomogeneous elastic media, *Wave Motion* **3**, 1 (1984).
  - [2] C. F. Sieck, A. Alù, and M. R. Haberman, Origins of Willis coupling and acoustic bianisotropy in acoustic metamaterials through source-driven homogenization, *Phys. Rev. B* **96**, 104303 (2017).
  - [3] G. W. Milton and J. R. Willis, On modifications of Newton's second law and linear continuum elastodynamics, *Proc. R. Soc. A* **463**, 855 (2007).
  - [4] A. N. Norris, A. L. Shuvalov, and A. A. Kutsenko, Analytical formulation of 3D dynamic homogenization for periodic elastic systems, *Proc. R. Soc. A* **468**, 1629 (2012).
  - [5] M. B. Muhlestein, C. F. Sieck, A. Alù, and M. R. Haberman, Reciprocity, passivity and causality in Willis materials, *Proc. R. Soc. A* **472**, 20160604 (2016).
  - [6] M. B. Muhlestein, C. F. Sieck, P. S. Wilson, and M. R. Haberman, Experimental evidence of Willis coupling in a one-dimensional effective material element, *Nat. Commun.* **8**, 15625 (2017).
  - [7] S. Koo, C. Cho, J.-H. Jeong, and N. Park, Acoustic omni meta-atom for decoupled access to all octants of a wave parameter space, *Nat. Commun.* **7**, 13012 (2016).
  - [8] H. Nassar, X. C. Xu, A. N. Norris, and G. L. Huang, Modulated phononic crystals: Non-reciprocal wave propagation and Willis materials, *J. Mech. Phys. Solids* **101**, 10 (2017).

- [9] Y. Liu, Z. Liang, J. Zhu, L. Xia, O. Mondain-Monval, T. Brunet, A. Alù, and J. Li, Willis Metamaterial on a Structured Beam, *Phys. Rev. X* **9**, 011040 (2019).
- [10] Y. Chen, X. Li, G. Hu, M. R. Haberman, and G. Huang, An active mechanical Willis meta-layer with asymmetric polarizabilities, *Nat. Commun.* **11**, 3681 (2020).
- [11] J. Li, C. Shen, A. Diaz-Rubio, S. A. Tretyakov, and S. A. Cummer, Systematic design and experimental demonstration of bianisotropic metasurfaces for scattering-free manipulation of acoustic wavefronts, *Nat. Commun.* **9**, 1342 (2018).
- [12] L. Quan, Y. Ra'di, D. L. Sounas, and A. Alù, Maximum Willis Coupling in Acoustic Scatterers, *Phys. Rev. Lett.* **120**, 254301 (2018).
- [13] S. R. Craig, X. Su, A. Norris, and C. Shi, Experimental Realization of Acoustic Bianisotropic Gratings, *Phys. Rev. Appl.* **11**, 061002(R) (2019).
- [14] Z. Hou, X. Fang, Y. Li, and B. Assouar, Highly Efficient Acoustic Metagrating with Strongly Coupled Surface Grooves, *Phys. Rev. Appl.* **12**, 034021 (2019).
- [15] Y. Fu, C. Shen, Y. Cao, L. Gao, H. Chen, C. T. Chan, S. A. Cummer, and Y. Xu, Reversal of transmission and reflection based on acoustic metagratings with integer parity design, *Nat. Commun.* **10**, 2326 (2019).
- [16] Y. K. Chiang, S. Oberst, A. Melnikov, L. Quan, S. Marburg, A. Alù, and D. A. Powell, Reconfigurable Acoustic Metagrating for High-Efficiency Anomalous Reflection, *Phys. Rev. Appl.* **13**, 064067 (2020).
- [17] A. Merkel, V. Romero-García, J.-P. Groby, J. Li, and J. Christensen, Unidirectional zero sonic reflection in passive PT-symmetric Willis media, *Phys. Rev. B* **98**, 201102(R) (2018).
- [18] Y. Zhai, H.-S. Kwon, and B.-I. Popa, Active Willis metamaterials for ultracompact nonreciprocal linear acoustic devices, *Phys. Rev. B* **99**, 220301(R) (2019).
- [19] X. Bai, C. Qiu, H. He, S. Peng, M. Ke, and Z. Liu, Extraordinary lateral beaming of sound from a square-lattice phononic crystal, *Phys. Lett. A* **381**, 886 (2017).
- [20] A. S. Titovich and A. N. Norris, Acoustic Poisson-like effect in periodic structures, *J. Acoust. Soc. Am.* **139**, 3353 (2016).
- [21] P. Gao, J. Sánchez-Dehesa, and L. Wu, Poisson-like effect for flexural waves in periodically perforated thin plates, *J. Acoust. Soc. Am.* **144**, 1053 (2018).
- [22] X. Su and A. N. Norris, Retrieval method for the bianisotropic polarizability tensor of Willis acoustic scatterers, *Phys. Rev. B* **98**, 174305 (2018).
- [23] X. Su and D. Banerjee, Extraordinary Sound Isolation Using an Ultrasparse Array of Degenerate Anisotropic Scatterers, *Phys. Rev. Appl.* **13**, 064047 (2020).